Available online at www.sciencedirect.com
ScienceDirect
Quaternary Research 68 (2007) 353–363
QUATERNARY RESEARCH
www.elsevier.com/locate/yqres

Relationships between glacier and rock glacier in the Maritime Alps, Schiantala Valley, Italy

Adriano Ribolini [a,*], Alessandro Chelli [b], Mauro Guglielmin [c], Marta Pappalardo [a]

[a] *Dipartimento di Scienze della Terra, Università di Pisa, Pisa, via S. Maria 53, 56126 Pisa, Italy*
[b] *Dipartimento di Scienze della Terra, Università di Parma, Viale G.P. Usberti 157 A, 43100, Parma, Italy*
[c] *Dipartimento di Biologia Strutturale e Funzionale, Università dell'Insubria, via H. J. Dunant, 3, 21100 Varese, Italy*

Received 29 September 2006

Abstract

In the Schiantala Valley of the Maritime Alps, the relationship between a till-like body and a contiguous rock glacier has been analyzed using geomorphologic, geoelectric and ice-petrographic methodologies. DC resistivity tomographies undertaken in the till and in the rock glacier show the presence of buried massive ice and ice-rich sediments, respectively. Ice samples from a massive ice outcrop show spherical gas inclusions and equidimensional ice crystals that are randomly orientated, confirming the typical petrographic characteristics of sedimentary ice. The rock glacier formation began after a phase of glacier expansion about 2550±50 ^{14}C yr BP. Further ice advance during the Little Ice Age (LIA) overrode the rock glacier root and caused partial shrinkage of the pre-existing permafrost. Finally, during the 19th and 20th centuries, the glacial surface became totally debris covered. Geomorphological and geophysical methods combined with analyses of ice structure and fabric can effectively interpret the genesis of landforms in an environment where glaciers and permafrost interact. Ice petrography proved especially useful for differentiating ice of past glaciers versus ice formed under permafrost conditions. These two mechanisms of ice formation are common in the Maritime Alps where many sites of modern rock glaciers were formerly occupied by LIA glaciers.

Keywords: Rock glacier; Debris-covered glacier; Glacier; Permafrost; DC resistivity; Ice petrography; Holocene; Maritime Alps

Introduction

The debate on the relationship between rock glaciers and glaciers has mainly focused on whether or not the two landforms could be genetically linked (for a summary, see Whalley and Martin, 1992; Whalley and Azizi, 1994). Some authors state that all of the valley-floor developing rock glaciers (as opposed to valley-side rock glaciers) are strictly permafrost creep phenomena that lack genetic relations with the glacial snout (Haeberli, 1985; Barsch, 1992). Conversely, other authors document the existence of glacigenic rock glaciers that are significantly cored by sedimentary ice and mantled by a continuous and relatively thin debris cover (Potter, 1972; Humlum, 1996; Potter et al., 1998; Krainer and Mostler, 2000; Krainer et al., 2002). A continuum between debris-free glaciers and rock glaciers has also been proposed to support a possible glacial origin of rock glaciers, with debris-covered glaciers as an intermediate stage (Clark et al., 1994; Ackert, 1998; Shroder et al., 2000; Berger et al., 2004).

In recently deglaciated forefields, namely those once occupied by Little Ice Age (LIA) glaciers, the situation could be more complicated. Here, advances of LIA glaciers locally caused the covering of pre-existing permafrost by the glacier snout, indicating the coexistence of congelation and sedimentary ice within the same detrical body (Haeberli and Vonder Mühll, 1996; Reynard et al., 2003; Kneisel, 2004; Lugon et al., 2004; Kääb and Kneisel, 2006). Thus, there is a need to improve knowledge about the rock glacier–glacier relationship, especially with regard to providing data for an integrated approach to sites where buried ice is exposed or where it has been cored. Distinguishing debris-covered glaciers from rock glaciers is

* Corresponding author.
E-mail addresses: ribolini@dst.unipi.it (A. Ribolini), alessandro.chelli@unipr.it (A. Chelli), mauro.guglielmin@uninsubria.it (M. Guglielmin).

0033-5894/$ - see front matter © 2007 University of Washington. All rights reserved.
doi:10.1016/j.yqres.2007.08.004

important because they are both indicators of climate but respond differently to environmental changes (Haeberli, 1990).

This distinction is particularly needed in the Maritime Alps, where glaciers have extensive areas of their surface covered by debris (Federici and Pappalardo, 1995) and buried massive ice lenses have been identified in some rock glaciers and recently deglaciated areas (Evin and Fabre, 1990; Bianchi et al., 2004). The Schiantala Valley (upper Stura di Demonte Basin, Maritime Alps) is emblematic of these geomorphological situations. Here, massive foliated ice outcrops beneath a few decimeters of debris on the side of a depression opening into a cirque floor. From the downvalley border of this depression, a rock glacier extends about 600 m downvalley. In this area, Camoletto (1931) described the Schiantala Glacier as completely debris covered, with clean ice visible only in two plates near the base of the cirque wall and beneath the debris exposed in the wall of a big crevasse. The debris-covered glacier observed by Camoletto (1931) was interpreted as a rock glacier by Evin (1993), indicating that melting processes of ice-rich permafrost/ground ice explained the depression formation. In both cases, the nature of the associated ice was not investigated and the landform interpretations were based only on surface morphological features. In such a situation, analysis of ice microstructural characteristics can be used to provide information about the genetic origin of the ice because crystal shape and orientation are different between sedimentary and permafrost ice (Duval, 1981; Patterson, 1994).

We believe that the Schiantala Valley is a particularly suitable site to obtain insight into rock glacier–glacier relationships in a recently deglaciated area. The aims of the study are (i) to define the nature of massive ice covered by debris and (ii) to detect and interpret the presence of ice-rich sediments inside the rock glacier. Here, a detailed mapping of glacial/periglacial landforms, chronologically constrained, allow us to reconstruct the dynamic relationships between a rock glacier and a retreating glacier.

General setting

The Maritime Alps are located 50 km north of the Mediterranean Sea (Fig. 1). High-grade metamorphic rocks of the Argentera crystalline Massif characterize the basement outcrop. Several phases of glacial advance during the Pleistocene and Holocene characterized the landscape of the

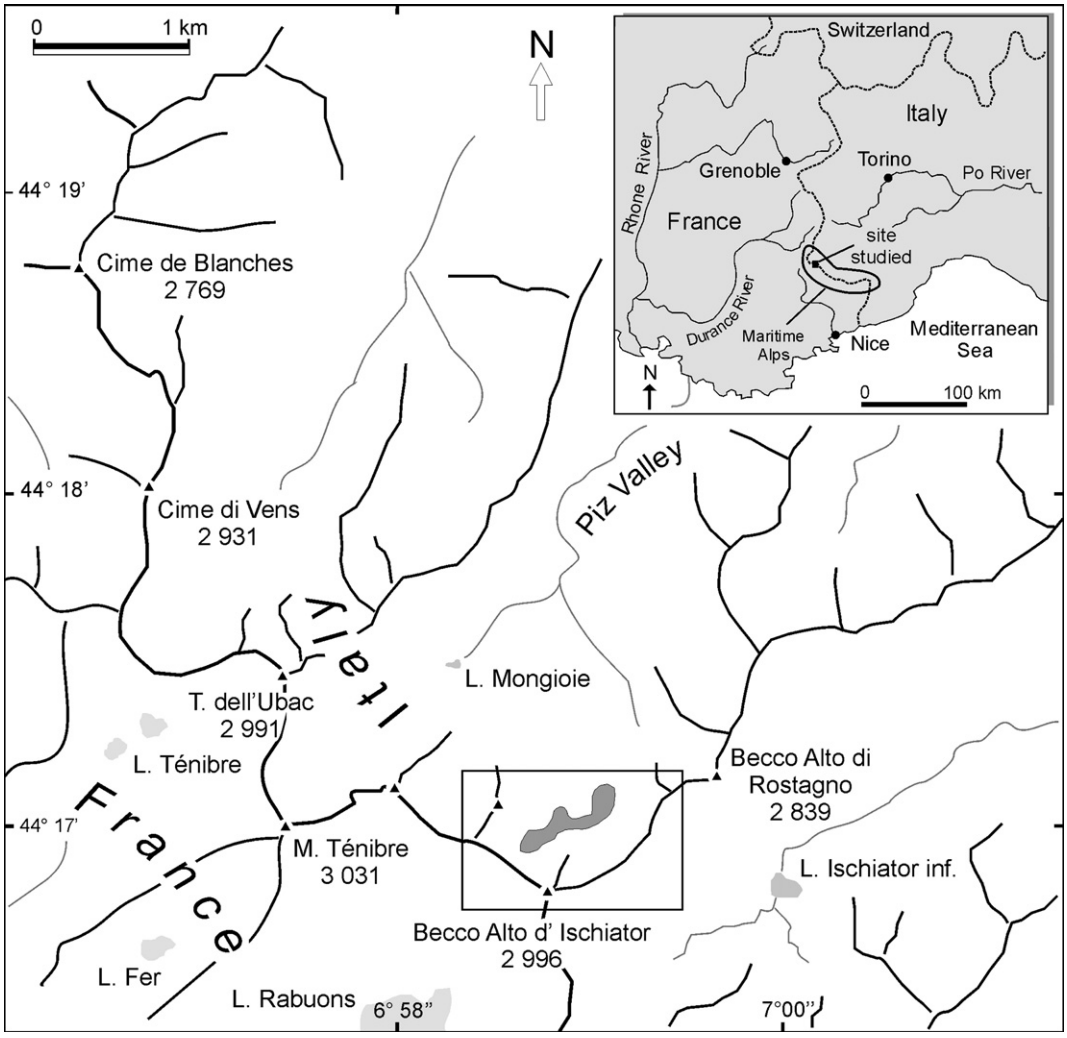

Figure 1. Regional sketch map of the studied area. Schiantala rock glacier in dark grey.

https://doi.org/10.1016/j.yqres.2007.08.004 Published online by Cambridge University Press

Maritime Alps (Federici and Pappalardo, 1995; Federici and Stefanini, 2001; Finsinger and Ribolini, 2001; Federici et al., 2003). Today, only a few glaciers exist in the southeastern part of the Maritime Alps (Gesso basin); they underwent an intense retreat during the last decades of 20th century and today are experiencing accelerated processes of debris covering (Pappalardo, 1999; Bianchi et al., 2004). In the Stura di Demonte basin, the last glaciers disappeared during the final decades of the 20th century (Federici and Pappalardo, 1995; Pappalardo, 1999). Although the Schiantala Glacier was declared extinct between AD 1959 and 1961 (Consiglio Nazionale delle Ricerche-Comitato Glaciologico Italiano, 1959–1961), it was subsequently classified as "regenerated" in the World Glacier Inventory (IAHS, UNEP, UNESCO, 1989).

More than 160 rock glaciers have been mapped in the Maritime Alps (Schweitzer, 1968; Smiraglia and Guglielmin, 1997; Ribolini, 1999). The rock glaciers above an altitude of 2600 m are believed to be active, with an average thickness of permafrost layer often exceeding tens of meters (Ribolini, 2001; Ribolini and Fabre, 2006). Between an altitude of 2500 m and 2600 m, the rock glacier permafrost is probably near its climatic limit for existence, with a thickness of <6 m to 7 m and temperature near the melting point.

Study area

The Schiantala Valley is characterized by a glacial cirque in its upper part and it terminates downward into a glacial-scoured depression that is bordered by a step at an altitude of about 2460 m (Fig. 2). The depression floor is partly filled by glacial deposits, both shaped as moraine ridges and chaotic accumulations that likely correspond to supra-glacial and/or melt-out

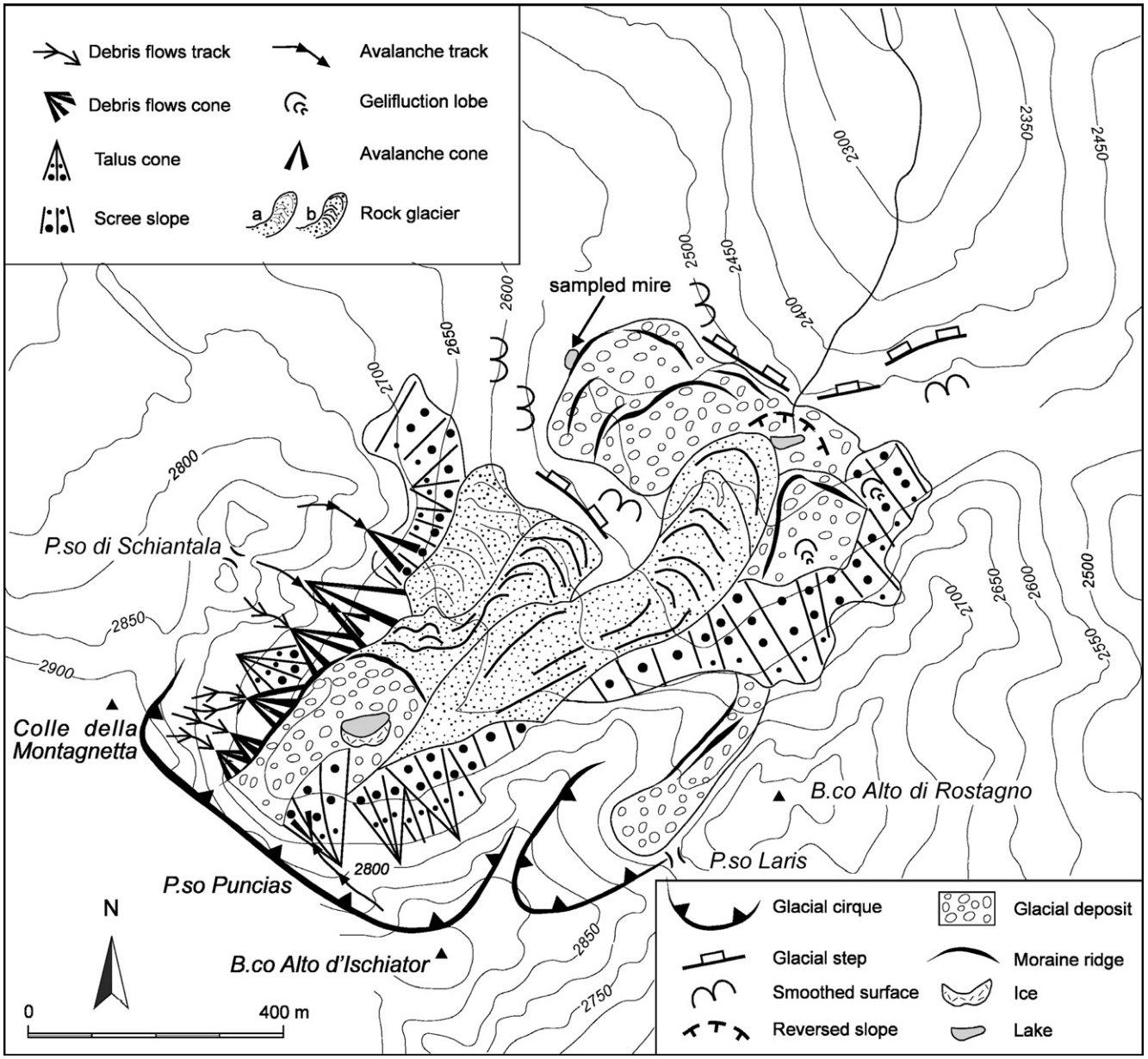

Figure 2. Geomorphologic sketch map of the upper Schiantala Valley. Location of sampled mire is reported.

https://doi.org/10.1016/j.yqres.2007.08.004 Published online by Cambridge University Press

Figure 3. Area of frontal moraines in the proximity of the rock glacier front. Radiocarbon dates from sampled mire are reported.

debris. In the proximity of the NW margin of the depression, a sequence of small moraine ridges is observed. A lateral and end moraine of this sequence dams the water flow forming a mire and providing a suitable site to date organic material that accumulated prior to the corresponding glacial advance (Fig. 3).

In the uppermost part of the cirque, a lateral moraine lies at an altitude between 2690 m and 2750 m, and an end moraine crosses the valley at an altitude of 2690 m (Fig. 2). Upvalley from this ridge, a depression is formed in a till that is characterized by a highly variable grain size from pebbles to boulders locally exceeding 3 m in diameter. Currently, a lake of about 3000 m^2 occupies part of this depression. Along the southern side of the lake, massive ice outcrops beneath a few decimeters of a blocky layer of till (Fig. 4).

Downvalley of this area, re-worked till sediments continue to dominate the composition of the two rock glaciers. The biggest rock glacier, here referenced as "Schiantala rock glacier", has a tongue-shape morphology and extends from the cirque threshold to the glacial hollow at an altitude of 2470 m (Fig. 5, see also Fig. 2). It is composed mainly of boulders with maximum diameters often exceeding 3 meters. The surface is very dense with flow features, such as transverse/longitudinal ridges and trenches, as well as conical pits and funnel-shaped hollows. The surface texture of these flow features allows identification of two main flow units (U1, U2) within the rock glacier, which has a bilobate form (Fig. 5). The U1 flow unit extends from the upper to the lower part of the Schiantala rock glacier, showing a gradual change from a surface characterized by longitudinal ridges to a surface dominated by transverse concentric ridges. The front is steep (>30°) and enters a small lake (Laris Lake) at an altitude of 2470 m. The U2 flow unit corresponds to a few concentric ridges visible in the central-western part of the rock glacier. The U2 flow unit extends downvalley to the cirque threshold at an altitude of 2600 m, where a steep 4- m to 5-m-high front is visible. U1–U2 geometrical relationships are not very clear, although the external longitudinal ridge of U1 does seem to cut the concentric ridges of U2. The absence of vegetation on the surface and the sporadic lichen cover suggest that the Schiantala rock glacier is active in most of its parts.

Adjacent to the northwest side of the Schiantala rock glacier, a small rock glacier was identified which is partly covered by a debris cone (Fig. 2). Its surface flow features are poorly preserved and only a few concentric ridges are visible. The blocks that constitute the deposit are more weathered than those of the Schiantala rock glacier.

In the Schiantala Valley, Camoletto (1931) described a glacier that extended from the base of the cirque wall at 2720 m to an altitude of about 2670 m. Here, the glacier was divided into two

Figure 4. Massive ice outcrop in the cirque floor at 2690 m. The dip of the foliation of ice ranges between 12 and 48°.

https://doi.org/10.1016/j.yqres.2007.08.004 Published online by Cambridge University Press

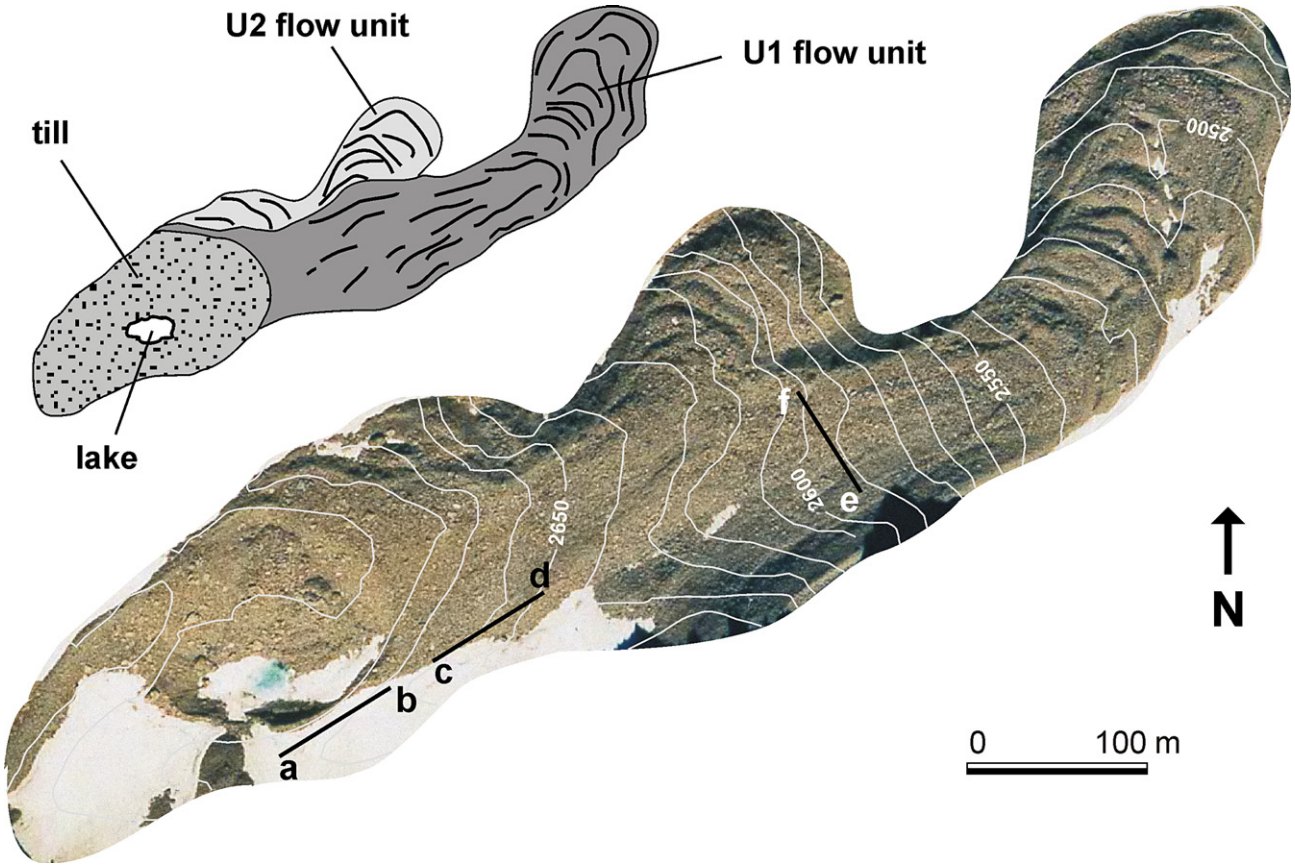

Figure 5. Aerial image and interpretation of glacier and rock glacier deposits in the topmost part of the Schiantala Valley. The position of geoelectrical tomographies is shown and a–b, c–d and e–f letters identify profiles extremes in Figures 7a–c.

minor snouts, both possibly reaching an altitude of 2600 m. Two clean-ice plates were visible near the base of the cirque wall, and clean ice cropped out beneath the debris in the wall of a large crevasse (Camoletto, 1931). Evidences from the 1931 field observations indicates that during the LIA maximum the glacier covered both the depression where today the massive ice crops out and the mid- to upper part of the Schiantala rock glacier.

Methods

Sediment dating

In order to chronologically constrain the glacial evolution of the valley, a trench (S1) and 5 boreholes (S2–S6) were dug in a mire deposit sustained by a lateral–frontal moraine. The boreholes, carried out with a handcorer that was 15 cm long and 4 cm in diameter, reached the basement at a depth of 50 cm. All of the sediments were described with Munsell color charts, and grain size was estimated. Organic sediments were extracted from two undisturbed samples of S1 trench and S6 core. These sediments were AMS radiocarbon dated (Beta Analytic).

Electrical DC resistivity sounding

DC resistivity tomography was used to detect the presence and the type of subsurface ice (e.g., Hauck et al., 2003). In this study, an IRIS SYSCAL R1 Georesistivity Meter and two multi-conductor cables equipped with 48 electrodes were used. The technical specifications of this device, above the 10-MΩ input impedance, were particularly suitable for this kind of investigation. Both Wenner and double-dipole electrode arrays spaced 2 m apart were used. The first array allows high penetration depth of injected current, while the second provides a greater lateral resolution (Telford et al., 1990). The Wenner survey acquisition was programmed for 360 measurements, with $n=15$ levels. The dipole–dipole survey acquisition was programmed for 255 measurements, with $n=6$ levels (the number of levels was limited because of the high error expected for deeper levels). Salt water was added to the electrodes to improve the contacts with the coarse ground. Data processing was carried out with the finite-elements software *TomoLab*, produced by Geostudi Astier s.r.l.. This software allows for simultaneous inversion of data obtained with the different electrode arrays. Surface topography was measured in the field using centimeter-gradated bars and was incorporated in the data inversion.

Ice sampling and analysis

Samples were directly cut from the massive ice core outcrop with ice axes. The samples were placed in polyethylene bags after a macroscopic description and were stored in a cold room at

https://doi.org/10.1016/j.yqres.2007.08.004 Published online by Cambridge University Press

−25 °C. Fourteen thin vertical sections (0.8 mm thick) were obtained in a cold room (at a temperature of −15 °C) in Milan II University (Teruzzi, 2000). All of the sections were photographed in normal and polarized light with a range of enlargements. For each thin section, the optical *C*-axes were determined according to the procedure reported in Langway (1958) and the results were plotted on Schmidt (equiareal, lower hemisphere) stereograms. Crystal size was determined by two different methods. The first method is that of the mean intercept (Thorsteinsson et al., 1995) in which the length of a test line drawn on a picture of the section is divided by the number of the crystals crossed, giving the crystal size *L*. The second method consists of direct measurements (DM) of the crystals with *L* greater than 5 mm. Both of the methods were applied along a horizontal (*X*) and vertical plane (*Z*). On the same images, we counted the gas bubbles, and using some comparison masks, we estimated the area and diameter of the bubbles greater than 1 mm and also recorded their type of shape (circular, elongated, pear-shaped).

Ela calculation

To outline the glacial episodes of the Schiantala glacier, the corresponding Equilibrium Line Altitude (ELA) was calculated by means of the balance ratio method (BR) (Furbish and Andrews, 1984) and the accumulation area ratio method (AAR) (Meier and Post, 1962). The BR method is the most suitable for snow-fed, clean glaciers, but it is inappropriate when a relevant proportion of the accumulation originated by avalanching and where debris cover exerts a strong influence on the ablation gradient. In the present work, a ratio between accumulation and ablation gradient of 1.6 was used. The AAR method provides appropriate value of the steady-state AAR when applied to clean, snow-fed glaciers as well as to avalanche-fed and debris-covered ones. Although the AAR method was deemed not appropriate here, the results obtained with BR and AAR methods are compared to evaluate the possible debris-covering effect on ELA values.

Results

Sediments dating

Locations of S1–S6 in the mire, the S1–S2–S3 lithostratigraphic correlation and their relationship with the lateral–frontal moraine are reported in Figure 6. Three clayey levels in the S1 sequence with different colors (10YR 3/3, 7.5YR 6/4, 2.5YR 4/4) overlap a till at a depth of 30 cm. The S2 sequence is characterized by four layers from top to bottom: 20 cm of dark brown clayey silt (10 YR 3/3), 15 cm of brown-dark brown clayey silt (7.5YR 4/4), 15 cm of dusky red silt (2.5YR 3/2) and 20 cm of black silt (2.5 YR 2/1) that is rich in organic content and overlies the bedrock. This basal organic-rich layer was dated by the AMS radiocarbon method at 2270±50 ^{14}C yr BP (Beta-181872).

Two clayey silt layers (10YR 3/3, 10YR 3/2) characterize the totality of the S3 sequence.

The boreholes from S3 to S6 indicate a progressive thickening of the deposit moving toward borehole S6, which is located in the most depressed part of the mire where shallow water is seasonally present (Fig. 6). In S6, a 30-cm layer of clayey silt (7.5 YR 2/0) was found below 40 cm of clay (10 YR 3/2). The organic mat of the basal layer was AMS radiocarbon dated at 2480±50 ^{14}C yr BP (Beta-181873).

Electrical dc resistivity sounding

Georesistivity tomographies were carried out along the right bank of the lake in the cirque floor, immediately downvalley of the depression at the root of the rock glacier, and crossing the central part of the rock glacier (Fig. 5). Results are reported in Figures 7a–c, respectively, illustrating the first 18–19 m of underground resistivity distribution. Bedrock was not reached in any sounding because the lowermost layers never presented a rapid decrease in resistivity up to the values typical of the Argentera Massif basement (about 10 kΩm) (Ribolini and

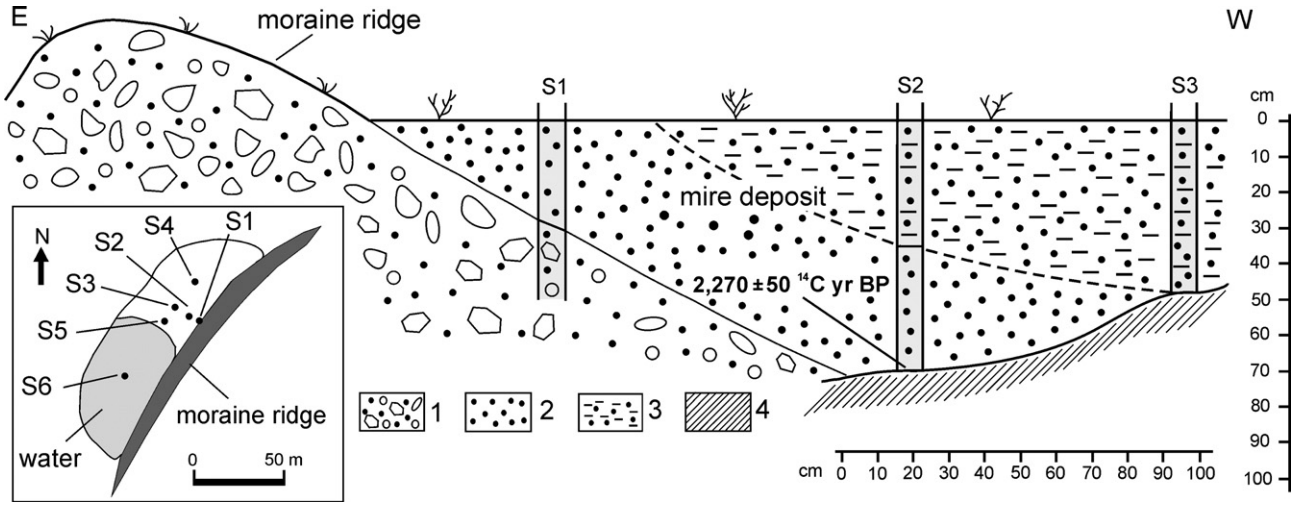

Figure 6. Reconstructed stratigraphic section in correspondence of the sampled mire at 2520 m. (1) massive diamicton sandy-gravel supported; (2) silt; (3) clayey silt; (4) bedrock.

https://doi.org/10.1016/j.yqres.2007.08.004 Published online by Cambridge University Press

Fabre, 2006). An open-work surface layer composed of very large boulders was constantly observed in the field. This layer presents a variable thickness within the first 2–4 m of depth. The relative resistivity is generally lower than 15 kΩm in the rock glacier and is much higher (100–300 kΩm) near the bank of the lake.

In the tomography done near the lake (Fig. 7a), an apparent three-layer structure is evident, with increasing resistivity values with depth from 100–200 kΩm up to 4–5 MΩm. Layer boundaries appear subhorizontal and are relatively well defined. Laterally, the deepest layer gradually decreases its resistivity moving northeast, approaching the depression border.

The tomography at the rock glacier root (Fig. 7b) can be divided into two parts. The downvalley part (to NE) shows a wide upper layer (2–12 m depth) with resistivities of 10–20 kΩm, locally interrupted by subcircular spots exceeding 30–40 kΩm. Resistivity progressively increases with depth up to 15 m, where it constantly assumes values of >40 kΩm. High resistivities characterize the upvalley part (to SW) of the tomography. In particular to the extreme left, a high resistivity layer (0.6 MΩm) is found below 2–5 m of the medium resistivity layer (80–100 kΩm). This high-resistivity layer terminates downvalley with a sharp edge extending beneath the maximum depth of investigation. Moving toward the center of the tomography, a layer constantly ranging between 90 and 100 kΩm is present, which is interrupted by a lenticular spot >170 kΩm at 6–10 m depth. Such a resistivity distribution is very similar to that found in the central part of the rock glacier

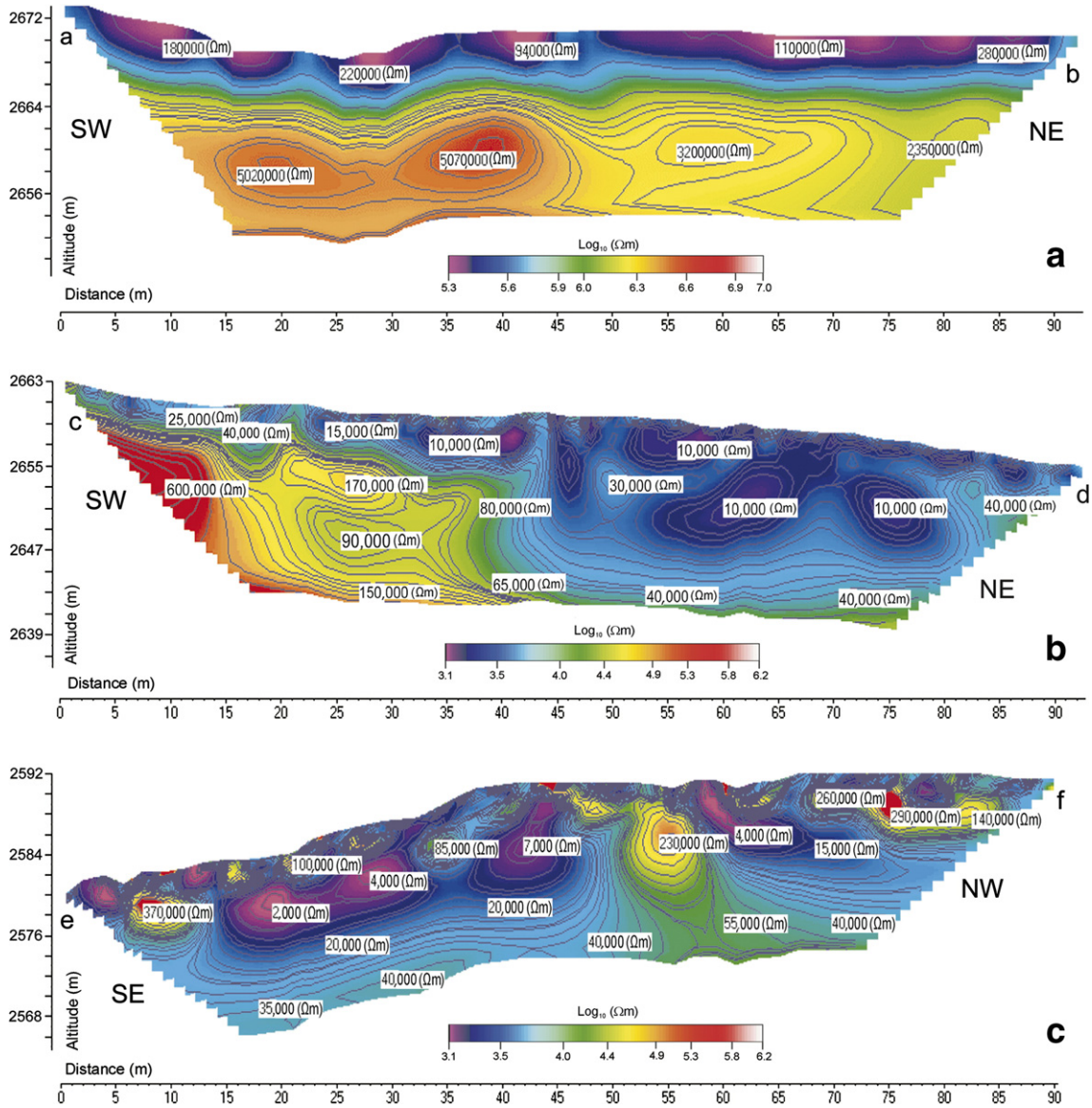

Figure 7. Geoelectrical tomographies undertaken along the right bank of the lake in the cirque floor (a), at the root of the rock glacier (b) and crossing the central part of the rock glacier (c). Results of the simultaneous inversion of the data obtained with the Wenner and dipole–dipole arrays are reported; a–b, c–d and e–f letters correspond to the geoelectrical tomographies orientation on Figure 5.

https://doi.org/10.1016/j.yqres.2007.08.004 Published online by Cambridge University Press

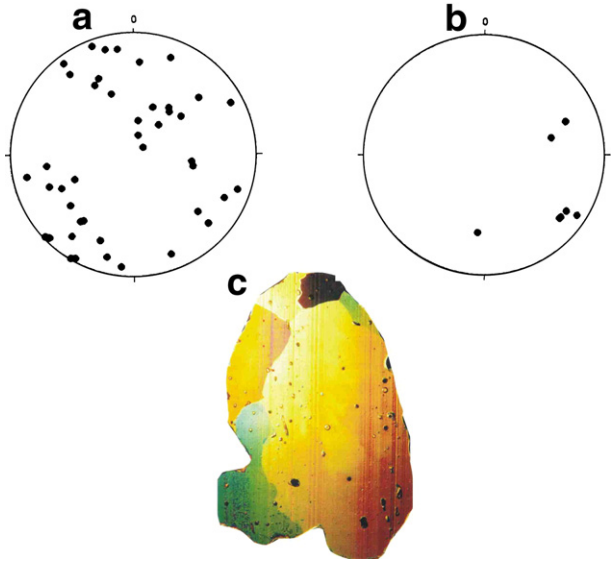

Figure 8. Schmidt diagrams of *C*-axis of ice crystal at different depths (245 cm and 700 cm, respectively, in panels a and b). The picture shown in panel c is the thin section correspondent to the Schmidt diagram in panel b.

(Fig. 7c), where a medium-low resistivity layer (2–4 kΩm) is interrupted by isolated spots higher than 200 kΩm.

Massive ice analysis

The outcrop of massive ice along the southern shoreline of the lake is stratified as shown in Figure 4, with debris layers differently dipping according to a synform ranging between 12° and 48°. The ice appears very bubbly, with mainly spherical gas inclusions (up to 5 mm in diameter) in the upper layers (down to 2.5 m depth). At increased depth, the ice is clearer and presents larger and elongated bubbles (up to 15 mm) that are generally parallel to the dip of the debris layers. Ice crystal diameters range between 3.1 and 82.2 mm, with the upper layers characterized by crystals of smaller size (3.1–8.8 mm) against the deeper ones that show coarser crystals (8.8–82.2 mm). Almost all of the crystals are equidimensional with a ratio between the vertical diameter (d_V) and the horizontal diameter (d_O) of around 1 (ranging between 0.9 and 1.3), even for some slightly elongated crystals in the deeper layers. The *C*-axes of the crystals are randomly orientated in all of the thin sections with an inclination that is generally parallel to or slightly higher than the debris layers (Fig. 8).

Discussion

Buried ice/ground ice relationships

The tomographies show the passage from an area where extreme resistivities are dominant and distributed in regular subhorizontal beds (Fig. 7a) to an area characterized by generally lower resistivity values with some relatively high resistivity spots (Fig. 7c). According to the previous literature (i.e., Evin and Fabre, 1990; Haeberli and Vonder Mühll, 1996), the very high resistivity values found in the upper part of the studied area (Fig. 7a) should be related to a massive sedimentary ice core below a 1- to 2-m-thick debris layer. In addition, the microscopic analysis shows that both the size and *C*-axes orientations of the crystals are consistent with a sedimentary origin of the ice. This becomes more evident with samples that are collected from deeper sites (Fig. 8).

Geomorphological data and the microscopic analyses of the massive ice demonstrate that the upper part of the area can be considered a debris-covered glacier, in contrast with what was previously hypothesized by Evin (1993). Consequently, the depression occupied by the lake results from a glacial-karst process affecting this buried massive ice.

The resistivity values shown in the tomography at the rock glacier root (Fig. 7b) should be related to large variations of ice content in the sediments (e.g., King et al., 1987; Evin and Fabre, 1990; Haeberli and Vonder Mühll, 1996). The shape of the tomography structure also suggests that the high resistivity values of the left upper part of the tomography have to be associated with massive sedimentary ice, as found in other rock glaciers (Guglielmin et al., 2004). The sharp and very steep contact between high resistivity values (0.6 MΩm) and relatively more conductive sediments downvalley of the depression corresponds to a sector where geomorphological mapping suggests a possible transition from a frontal morainic ridge to a rock glacier (Fig. 5). In this transitional area, we must take into account the possible effect of a glacier margin extending farther downvalley to the point of covering the rock glacier root. The consequent modification of the ground thermal regime and the presence of meltwater circulation induced a process of degradation of the subglacial and proglacial pre-existing permafrost.

The resistivity values in the lowest part of tomography 2 and tomography 3 (Figs. 7b, c) also could be related to sedimentary ice in ablation areas, according some authors (e.g., Guglielmin et al., 1995). However, the resistivity contour pattern suggests an internal structure composed of an ice–rock mixture in variable proportion, with local spots of high ice content. Accordingly, the surface flow features (Fig. 5) are those characteristic of deformation and flow of ice-rich sediment, such as permafrost creep (Kääb and Vollmer, 2000).

The heterogeneous distribution of the resistivity evident in the lowest part of tomography 2 and in tomography 3 could be explained in terms of an altitude variation in thermal conditions of the permafrost. As documented by Ribolini and Fabre (2006), cold ice-rich permafrost and warm permafrost can be found within the same rock glacier in the 2500- to 2600 m elevational belt of the Maritime Alps.

Alternatively, the subcircular structures characterized by a rapid increase/decrease of resistivity could be explained in terms of geothermal behavior and flow dynamics of the rock glacier, assuming a thermo-mechanical model of permafrost creep (for the details of the model, see Haeberli and Vonder Mühll, 1996). According to this model, a longitudinal extension generates a thinning in the ice-debris layer that, in turn, induces a thermal readjustment as a consequence of climatic control at the surface. This thermal readjustment tends to destabilize the high-resistive ice at the top of permafrost, which is

https://doi.org/10.1016/j.yqres.2007.08.004 Published online by Cambridge University Press

progressively replaced by ice with low resistivity or temperature near the melting point.

Some geomorphological features call for a potential applicability of this model to the Schiantala rock glacier. The decreasing resistivity passing from the higher to the lower half of tomography 2 (Fig. 7b) at the rock glacier root could be related to the onset of extensional flow dynamics as documented by the surface morphology. The southeast side of tomography 3 (Fig. 7c) crosses extensional flow features indicated by surface longitudinal ridges and furrows. Here, the resistivity distribution is compatible with destabilized permafrost, with isolated spots of high resistivity representing permafrost zones not yet replaced by low-resistivity ice.

Glacier–rock glacier dynamic relationships

The glacial advance documented by the frontal moraine at 2450 m can be dated by the minimum age "post quem" inferred from dating of the deepest basal peat (2480±50 ^{14}C yr BP, Beta-181873) from borehole S6 (Fig. 9a). This age corresponds to the Subboreal advance phase, which affected most glaciers in the Alps during the middle to late Holocene and earlier than the Little Ice Age (Orombelli and Pelfini, 1985; Baroni and Orombelli, 1996). Both AAR and BR methods used for the ELA calculation report a value of about 2620 m.

Considering the geomorphological evidence, the degree of weathering of the blocks and the absence in the Maritime Alps of other documented Holocene glacial advances younger than 2500 yr BP (Federici and Stefanini, 2001), the moraine at 2690 m apparently represents the LIA glacial expansion in this valley (Fig. 9c). The ELA value calculated with the AAR method (2650 m) is more realistic than obtained with the BR method (2689 m) because it is probable that during the LIA the Schiantala glacier was at least partly covered by debris.

The ELA shift between the 2480±50 ^{14}C yr BP advance and the LIA advance (30–70 m) is in agreement with that accounted for in the Maritime Alps (Puccioni, 2005) and reported for other parts of the world (e.g., the Norwegian Alps; Matthews et al., 2005).

The whole Schiantala rock glacier formed during the Subatlantic, surely after 2480±50 ^{14}C yr BP, deforming the till of the former Subboreal glacier (Fig. 9b). Considering the time needed for permafrost formation and the time required for permafrost creep, the only possible cold phase is the period around 1250–1050 ^{14}C yr BP when a glacial advance is reported for the western Alps (Orombelli and Porter, 1982). The

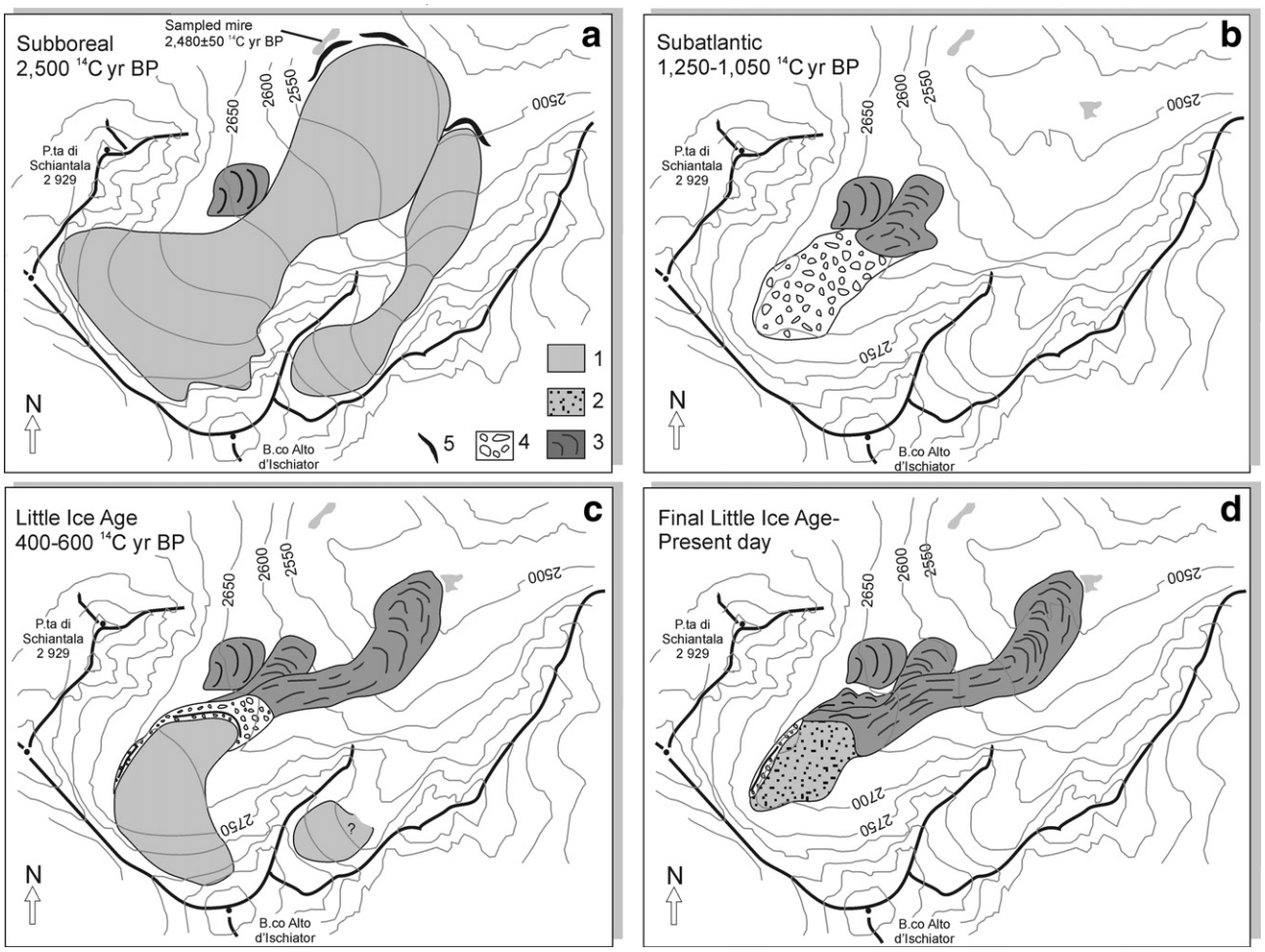

Figure 9. Cartoon reconstructing the relations between the glacier fluctuations and the rock glacier development during the late Holocene. (1) clean glacier; (2) debris-covered glacier; (3) rock glacier; (4) till; (5) moraine ridge.

https://doi.org/10.1016/j.yqres.2007.08.004 Published online by Cambridge University Press

subsequent LIA phase provided a new strong impulse to the permafrost creep (Fig. 9c). Accordingly, in the tomography at the rock glacier root, the sharp edge limiting the high resistivity layer (0.6 MΩm) can be interpreted as (i) the downvalley termination of a sedimentary ice layer or (ii) a fragment of sedimentary ice embedded in a syngenetically aggrading permafrost. In any case, the subsurface pattern of electrical resistivity implies the presence of a sedimentary ice layer protruding into the rock glacier root (Fig. 7b). This protrusion probably represents the LIA glacier advance that overlapped the apex of an existing rock glacier as already described in the Swiss Alps (Haeberli, 1985), in the Italian Central Alps (Guglielmin et al., 2001) and in the Pyrenees (Lugon et al., 2004).

Conclusion

Results of the present research shows how geomorphology, electrical resistivity and analyses of ice structure and fabric, combined with age assessments, can be integrated to differentiate debris-covered sedimentary ice from ice-rich permafrost and former permafrost that was buried by an advancing glacier now mostly melted.

During the Holocene, the Schiantala Valley landscape reacted to the global climatic oscillation with at least two glacial advances (Subboreal and Little Ice Age phases) and the formation of a complex rock glacier. Today, sedimentary ice covered by debris characterizes most of the cirque floor, and permafrost is present at least in the center-upper part of the rock glacier. Geomorphologic, geoelectrical and ice-petrographic analyses enabled us to reconstruct the dynamic relations between the rock glacier and the retreating glacier. Sediment dating fixed a starting point for this interaction.

The rock glacier began to develop from the ablation moraine complex progressively abandoned by the Schiantala glacier after 2550±50 ^{14}C yr BP. Permafrost aggradation could have started immediately after the retreat when creep of the permafrost layer led to the rock glacier formation. During the LIA phase, the Schiantala glacier advanced and overlapped the rock glacier root. Part of the pre-existing permafrost in this sector was degradated by subglacial and proglacial water circulation and by the heat flux induced by the covering glacier. Since the 19th–20th century, the glacial surface has become totally debris covered.

The modern studies undertaken on recently deglaciated areas have highlighted a complex ground ice distribution in such environments (Reynard et al., 2003; Kneisel, 2004; Kääb and Kneisel, 2006). The results of this paper confirm this scenario, showing how sedimentary and congelation ice can coexist at the same sites, due to the interaction between LIA glacier dynamics and rock glacier creep. Relicts of sedimentary ice buried by debris can be misinterpreted as ice-rich permafrost. Conversely, medium- to low-resistivity layers proximal to a former glacial margin can be misinterpreted as an ice–rock mixture undergoing a melting process, rather than correctly interpreted as a pre-existing permafrost disrupted by the advance of a glacier that is now melted out or debris covered. The results of this work are in agreement with the complex geomorphologic and paleoclimatic history reflected in the internal structure of other rock glaciers (e.g., Haeberli et al., 1999; Guglielmin et al., 2004; Lugon et al., 2004), where massive ice bodies within or superimposed on a permafrost layer have been found.

Acknowledgments

This research was supported by the Italian Ministry of University and Research within the framework of the Project COFIN 2005 “Increasing rate of Climate Change impacts on high mountain areas: cryosphere shrinkage and environmental effects”. Field work assistance by Geomorph Lab staff (University of Pisa) and geophysical advise by GeoLog (www.studiogeolog.it) were essential.

Suggestions and manuscript improving by M. O’Neal and J. C. Knox are highly acknowledged. The American Journal Experts staff (www.journalexperts.com/) improved the English text.

References

Ackert Jr., R.P., 1998. A rock glacier/debris-covered glacier system at Galena Creek, Absaroka Mountains, Wyoming. Geografiska Annaler A 80 (3–4), 267–276.

Baroni, C., Orombelli, G., 1996. The Alpine Iceman and Holocene climatic-change. Quaternary Research 46, 78–83.

Barsch, D., 1992. Permafrost creep and rock glacier. Permafrost and Periglacial Processes 11, 290–293.

Berger, J., Krainer, K., Mostler, W., 2004. Dynamics of an active rock glacier (Ötzal Alps, Austria). Quaternary Research 62, 233–242.

Bianchi, A., Ciuffi, P., D’Onofrio, L., Federici, P.R., Marchisio, M., Pappalardo, M., Ribolini, A., Sartini, S., 2004. Application of electrical resistivity tomography to investigation of buried ice and permafrost: two case studies from the Maritime Alps (Italy). Proceeding of European Geosciences Union. 1st General Assembly. Geophysical Research Abstract, vol. 6. Nice, France.

Camoletto, C.F., 1931. Le variazioni periodiche dei ghiacciai delle Alpi Marittime. Bollettino del Comitato Glaciologico Italiano ser.1, 11, 189–212.

Clark, D.H., Clark, M.M., Gillespie, A.R., 1994. Debris-covered glaciers in the Sierra Nevada, California, and their implication for snowline reconstruction. Quaternary Research 41, 139–153.

Consiglio Nazionale delle Ricerche-Comitato Glaciologico Italiano, 1959–1961. Ghiacciai del Piemonte. Catasto dei Ghiacciai Italiani, vol. II:Torino, 324 pp.

Duval, P., 1981. Creep and fabric of polycrystalline ice under shear and compression. Journal of Glaciology 27, 129–140.

Evin, M., 1993. Glacier et Glacier Rocheux dans les vallons de Mongioie et de Schiantala. Une nouvelle interprétation. Zeitschrift für Gletscherkunde und Glazialgeologie 27/28, 1–10.

Evin, M., Fabre, D., 1990. The distribution of permafrost in rock glaciers of Southern Alps (France). Geomorphology 3, 57–71.

Federici, P.R., Pappalardo, M., 1995. L’evoluzione recente dei ghiacciai delle Alpi Marittime. Geografia Fisica e Dinamica Quaternaria 18, 257–269.

Federici, P.R., Stefanini, M.C., 2001. Evidences and chronology of the Little Ice Age in the Argentera Massif (Italian Maritime Alps). Zeitschrift für Gletscherkunde und Glazialgeologie 37, 35–48.

Federici, P.R., Pappalardo, M., Ribolini, A., 2003. Geomorphological map of Maritime Alps Natural Park and surroundings. Color map, 1:25,000, S.EL.CA, Firenze.

Finsinger, W., Ribolini, A., 2001. Late glacial to Holocene deglaciation of the Colle del Vei del Bouc-Colle del Sabbione Area (Argentera Massif, Maritime Alps, Italy-France). Geografia Fisica e Dinamica Quaternaria 24, 141–156.

https://doi.org/10.1016/j.yqres.2007.08.004 Published online by Cambridge University Press

Furbish, D.J., Andrews, J.T., 1984. The use of hypsometry to indicate long-term stability and response of valley glaciers to changes in mass transfer. Journal of Glaciology 30, 199–211.

Guglielmin, M., Nardo, A., Smiraglia, C., 1995. Lo spessore dei ghiacciai della Valfurva. Misurazioni tramite Sondaggi Elettrici Verticali. Neve e Valanghe 24, 58–67.

Guglielmin, M., Cannone, N., Dramis, F., 2001. Permafrost–glacial evolution during the Holocene in the Italian Central Alps. Permafrost and Periglacial Processes 12, 111–124.

Guglielmin, M., Camusso, M., Polesello, S., Valsecchi, S., 2004. An old relict glacier body preserved in permafrost environment: the Foscagno rock glacier (upper Valtellina, Italian Central Alps). Arctic, Antarctic, and Alpine Research 36, 108–116.

Haeberli, W., 1985. Creep of mountain permafrost: internal structure and flow of alpine rock glaciers. Mitteilungen der Versuchsanstalt für Wasserbau, Hydrologie und Glaziologie 77, 1–142 (Zürich).

Haeberli, W., 1990. Glacier and permafrost signals of 20th-century warming. Annals of Glaciology 99–101.

Haeberli, W., Vonder Mühll, D., 1996. On the characteristics and possible origins of ice in rock glacier permafrost. Zeitschrift für Geomorphologie NF Supplementband 104, 43–57.

Haeberli, W., Kääb, A., Wagner, S., Vonder Mühll, D., Geissler, P., Haas, J.N., Glatzel-Mattheier, H., Wagenbach, D., 1999. Pollen analysis and 14C age of moss remains in a permafrost core recovered from the active rock glacier Murtèl-Corvatsch, Swiss Alps: geomorphological and glaciological implications. Journal of Glaciology 45, 1–8.

Hauck, C., Vonder Mühll, D., Maurer, H., 2003. Using DC resistivity tomography to detect and characterize mountain permafrost. Geophysical Prospecting 51, 273–284.

Humlum, O., 1996. Origin of rock glaciers: observations from Mellemfjord, Disko Island, central West Greenland. Permafrost and Periglacial Processes 7, 361–380.

Kääb, A., Kneisel, C., 2006. Permafrost creep within a recently deglaciated glacier Forefield: Muragl, Swiss Alps. Permafrost and Periglacial Processes 17, 79–85.

Kääb, A., Vollmer, M., 2000. Surface geometry, thickness changes and flow fields on creeping mountain permafrost: automatic extraction by digital image analysis. Permafrost and Periglacial Processes 11, 315–326.

King, L., Fisch, W., Haeberli, W., Wächter, H.P., 1987. Comparison on resistivity and radio-echo soundings on rock glacier permafrost. Zeitschrift für Gletscherkunde und Glazialgeologie 23, 77–97.

Kneisel, C., 2004. New insights into mountain permafrost occurrence and characteristics in glacier forefields at high altitude through the application of 2D resistivity imaging. Permafrost and Periglacial Processes 15, 221–227.

Krainer, K., Mostler, W., 2000. Reichenkar rock glacier: a glacier derived debris-ice-system in the Western Stubai Alps, Austria. Permafrost and Periglacial Processes 11, 267–275.

Krainer, K., Mostler, W., Span, N., 2002. A glacier-derived, ice-cored rock glacier in the Western Stubai Alps (Austria): evidence from ice exposures and ground penetrating radar investigation. Zeitschrift für Gletscherkunde und Glazialgeologie 38, 21–34.

IAHS, UNEP, UNESCO, 1989. World Glacier Inventory, Teufen, Switzerland.

Langway Jr., C.C., 1958. Ice fabrics and the universal stage. U.S. Army Snow Ice and Permafrost Research Establishment, Wilmette, Illinois. Technical Report, 62. 15 pp.

Lugon, R., Delaloye, R., Serrano, E., Reynard, E., Lambiel, C., Gonzalez-Trueba, J.J., 2004. Permafrost and Little Ice Age glacier relationships, Posets Massif, Central Pyrenees, Spain. Permafrost and Periglacial Processes 15, 207–220.

Meier, M.F., Post, A.S., 1962. Recent variations in mass net budgets of glaciers in western North America. International Association of Hydrological Sciences Publication 58, 63–77.

Matthews, J.A., Berrisford, M.S., Dressera, P.Q., Nesjeb, A.S., Dahl, O., Bjunec, A.E., Bakke, J., John, H., Birksc, B., Liec, Ø., Dumayne-Peatyg, L., Barnett, C., 2005. Holocene glacier history of Bjørnbreen and climatic reconstruction in central Jotunheimen, Norway, based on proximal glaciofluvial stream-bank mires. Quaternary Science Reviews 24, 67–90.

Orombelli, G., Pelfini, M., 1985. Una fase di avanzata glaciale nell'Olocene superiore, precedente alla Piccola Glaciazione, nelle Alpi Centrali. Rendiconti Società Geologica Italiana 8, 17–20.

Orombelli, G., Porter, S.C., 1982. Late Holocene fluctuations of Brenva Glacier. Geografia Fisica e Dinamica Quaternaria 5, 14–37.

Pappalardo, M., 1999. Remarks upon the present-day condition of the glaciers in the Italian Maritime Alps. Geografia Fisica e Dinamica Quaternaria 22, 79–82.

Patterson, W.S.B., 1994. The physics of glaciers, Pergamon3rd Edition. Oxford: 480 pp.

Potter, N., 1972. Ice-cored rock glacier, Galena Creek, northern Absaroka Mountains, Wyoming. Geological Society of America Bulletin 83, 3025–3057.

Potter, N., Steig, E.J., Clark, D.H., Speece, M.A., Clark, G.M., Updike, A.B., 1998. Galena Creek rock glacier revisited—New observations on an old controversy. Geografiska Annaler 80A (3–4), 251–265.

Puccioni, E., 2005. La deglaciazione delle Alpi Marittime sulla base del calcolo delle linee di equilibrio dei ghiacciai stadiali. Unpublished Degree Thesis, University of Pisa, 128 pp.

Reynard, E., Lambiel, C., Delaloye, R., Devaud, G., Baron, L., Chapellier, D., Marescot, L., Monnet, R., 2003. Glacier/permafrost relationships in forefields of small glaciers (Swiss Alps). Proceedings 8th International Conference on Permafrost, Zurich, Switzerland, Balkema, 2, pp. 947–952.

Ribolini, A., 1999. Areal distribution of rock glaciers in the Argentera Massif (Maritime Alps) as a tool for recent glacial evolution reconstruction. Geografia Fisica e Dinamica Quaternaria 22, 83–86.

Ribolini, A., 2001. Active and fossil rock glaciers in the Argentera Massif (Maritime Alps): surface ground temperatures and paleoclimatic significance. Zeitschrift für Gletscherkunde und Glazialgeologie 37, 125–140.

Ribolini, A., Fabre, D., 2006. Permafrost existence in the rock glaciers of the Argentera Massif (Maritime Alps, Italy. Permafrost and Periglacial Processes 17, 49–63.

Schweitzer, G., 1968. Die Verbreitung der Blockgletscher in den französisch-italienischen Seealpen. Aktualgeomorphologische Studien im oberen Tinéetal. Zeitschrift für Geomorphologie, Supplement Band 6, 1–167.

Shroder, J.F., Bishop, M.P., Copland, L., Sloan, V.F., 2000. Debris-covered glaciers and rock glaciers in the Nanga Parbat Himalaya, Pakistan. Geografiska Annaler 82A (1), 17–31.

Smiraglia, C., Guglielmin, M. (Eds.), 1997. Rock Glaciers Inventory of Italian Alps. Archivio Comitato Glaciologico Italiano, vol. 3 (103 pp).

Telford, W.M., Geldart, L.P., Sheriff, R.E., 1990. Applied geophysics. Cambridge University Press, New York. (770 pp).

Teruzzi, M., 2000. Analisi chimiche e fisiche di ground ice nell'ambiente periglaciale polare e alpino. Esempi da Amorphous glacier (Antartide), Foscagno (Sondrio) e Pietraporzio (Cuneo). Unpublished Thesis, University of Milan, 174 pp.

Thorsteinsson, T., Kipfstuhl, J., Eicken, H., Johnsen, S., Fuhrer, K., 1995. Crystal size variations in Eemian-age ice from the GRIP ice core, Central Greenland. Earth and Planetary Science Letters 131, 381–394.

Whalley, W.B., Azizi, F., 1994. Models of flow of rock glaciers: Analysis, critique and a possible test. Permafrost and Periglacial Processes 5, 37–51.

Whalley, W.B., Martin, H.E., 1992. Rock glaciers: II models and mechanisms. Progress in Physical Geography 16, 127–186.